Aged Titania Nanoparticles: The Simultaneous Control of Local and Long-Range Properties

Giuseppe Cappelletti,*,† Carlo Ricci,‡ Silvia Ardizzone,† Claudia Parola,† and Alberto Anedda‡

Department of Physical Chemistry and Electrochemistry, University of Milan, Via Golgi 19, I-20133 Milan, Italy, and Department of Physics, University of Cagliari, s.p. no. 8, Km 0.700.09042 Monserrato (CA), Italy,

Received: October 21, 2004; In Final Form: January 12, 2005

TiO_2 nanoparticles are obtained by combining a sol−gel preparative route with hydrothermal aging steps, performed in mild conditions, of varying time lengths. Both aged and un-aged samples are thermally treated at 300 and 600 °C, for the same length of time. The crystal structures, the phase composition, and crystallite sizes are analyzed by powder X-ray diffraction. Raman spectra of anatase nanocrystals with average sizes of 7−10 nm are reported and the correlation between the Raman band shape of the main feature at 144 cm^{-1} and the crystallite size is discussed. Nitrogen physisorption by Brunauer−Emmett−Teller (BET) method is adopted to evaluate the particles surface area and mesopore size and size distribution. The role played by the hydrothermal step in affecting the physicochemical properties of the powders is discussed also with respect to the H_2O/TiO_2 interactions as apparent from Raman spectroscopy investigations of the O−H stretching range (3000−3800 cm^{-1}).

Introduction

Nanocrystalline TiO_2, in particular, the anatase polymorph, is a material of great technological interest, used in a variety of applications such as photovoltaic solar cells, gas sensors, photo electrodes, and electrochromic display devices.[1−10] In the case of photoelectrochemical applications, nanosized anatase particles are desired to provide a very large surface area and enhanced activity due to quantum confinement effects in the semiconductor space charge.[5,8−10] At the same time, a regular microstructure and a good crystallinity[5,10] are required to reduce the formation of electron traps, due to lattice imperfections, which might affect the charge transport mechanisms through the titania network.[4] Further, conditions of good surface hydroxylation are necessary to promote the oxide wettability and the interfacial reactivity.

Alternative synthetic methods, with respect to the classical high-temperature calcinations are, therefore, sought to comply with the demanding, divergent material requirements. In fact, the introduction of high-temperature stages, to promote crystallinity, frequently gives rise to particle agglomeration with severe loss of effective surface area; further, it may induce phase transformation and provoke removal of physi- and chemisorbed water.

Hydrothermal treatments represent an alternative to high-temperature calcinations to promote crystallization under milder conditions. Results are present in the literature relative to hydrothermal preparations aimed at obtaining either titania nanoparticles or TiO_2 thin films.[4,7,9−12]

In the present work, a procedure that combines hydrothermal treatments of variable time length performed in mild conditions, with a sol−gel route to obtain the titanium oxide hydrous precursor, is presented. The sol−gel approach, which allows compositional and microstructural tailoring through controlling the precursor chemistry and processing conditions, is essentially based on the hydrolysis and subsequent polycondensation of a titanium alkoxide. The water/alkoxide ratio is a key synthesis parameter to control the absolute and relative rates of nucleation and growth of the particles. High (150:100) water/alkoxide ratios in the reaction medium provoke an extensive hydrolysis of the alkoxide, favoring nucleation versus particle growth. Intermediate values of water/alkoxide ratios (about 50) were adopted in the preparation of the oxide precursor to avoid the formation of exceedingly small colloidal clusters. The sol−gel precursors were submitted to the aging treatment in solution and, for the sake of comparison, also to direct calcinations at 300 and 600 °C. The particles were characterized by XRD and Raman scattering. XRD reveals the long-range order of the material and gives average structural information within several unit cells, while Raman scattering as a local probe is very sensitive to crystallinity and microstructures. Raman spectroscopy was also employed to investigate the nature and extent of the water−oxide interactions in the different conditions of the particle preparations. The morphological features were analyzed by nitrogen physisorption.

Experimental Section

All the chemicals were of reagent grade purity and were used without further purification; distilled water passed through a Milli-Q apparatus was used to prepare solutions and suspensions.

Sample Preparation. The preparation of TiO_2 particles by the sol−gel technique was performed at room temperature as follows: a solution of 0.2 mol of $Ti(OC_3H_7)_4$ in 50 mL of propanol was stirred for 30 min at 300 rpm. Then 175 mL of Milli-Q water were added quickly, drop by drop. The slurry was stirred for 90 min to complete the hydrolysis.

* Authors to whom correspondence should be addressed. E-mail: giusepppe.cappelletti@unimi.it (G.C.), silvia.ardizzone@unimi.it (S.A.), ricci@alfis.dsf.unica.it (C.R.), aanedda@unica.it. (A.A.) Telephone: +390250314225 (G.C., S.A., C.P.). Fax: +390250314300 (G.C., S.A., C.P.). Telephone: +390706754755 (C.R., A.A.).

† University of Milan.

‡ University of Cagliari.

10.1021/jp045192p CCC: $30.25
Published on Web 02/18/2005

The dried xerogel powders were purified by centrifugation−resuspension cycles, and then powder fractions were submitted to hydrothermal treatment in water (t_{HG} = 80 °C, pH = 6), varying the aging time (t_{HG} = 72, 144, 552 h). After aging, the suspensions were filtered and dried again at 80 °C. No washing was performed after the aging because of the low ionic strength of the aging solutions.

The samples are labeled as follows: TO represents titanium dioxide, HG, hydrothermal treatment. For example, TOHG552 is a precursor aged for 552 h. The precursor is labeled TO.pre.

Finally, the powders were thermally treated at 300 and 600 °C for 6 h under an oxygen stream.

Sample Characterization. Structural characterization of the powders was performed by X-ray diffraction using a Siemens D500 diffractometer, with Cu Kα radiation in the 10−80° 2θ angle range. The fitting program of the peaks was a particular Rietveld program[12,13] named QUANTO,[14] devoted to the automatic estimation of the weight fraction of each crystalline phase in a mixture.

The peak shape was fitted using a modified Pearson VII function. The background of each profile was modeled using a six-parameter polynomial in $2\theta^m$, where m is a value from 0 to 5 with six refined coefficients. When the mixture contains a certain percentage of amorphous particles, the Chebyshev function is used.

The mean dimension, d, of crystallites was obtained by elaborating the most intense X-ray peak of each phase by Scherer's equation,

$$d = \frac{K\lambda}{\beta \cos \theta}$$

where K is a constant related to the crystallite shape (0.9), β is the pure breadth of the powder reflection free of the broadening due to instrument contributions. This calibration was performed by means of the spectrum of a standard Si powder. The accurancy with which the Scherer's equation can be applied is limited by the uncertainties in K and by the success with which β can be deduced from the experimentally observed breadth. This equation is quite satisfactory for studies comparing the crystallite sizes of a number of samples belonging to a related series.

The method yields exhaustive values of the relative sizes even though the inflexible premises upon which the formula rests results in considerable uncertainty as to the absolute sizes.

"Calculated" surface areas have been obtained by elaborating the crystallite sizes obtained from X-ray diffraction spectra by means of the following formula:[18]

$$S_{calc} = \frac{6 \times 10^4}{d \times \rho}$$

ρ = average titanium oxide density (4.9 g cm^{-3});

d = crystallite diameter (Å).

The relation assumes that the particles are composed by single crystals, have a spherical geometry, and that both porosity and surface roughness are absent.

Consequently, this relation provides only approximate estimates of the surface area to be compared with the experimental one. Specific surface areas were determined by the classical Brunauer−Emmett−Teller (BET) procedure using a Coulter SA 3100 apparatus.

Micro Raman spectra (RS) have been collected in air at room temperature with a Raman spectrometer (Dilor XY800) operating with the 514.5 nm line of an argon ion laser (Coherent Innova 90C-4) in backscattering geometry. The signal, dispersed with a 1200 grooves/mm grating, was detected by a 1024 × 256 liquid nitrogen-cooled charge coupled detector (CCD), with a spectral resolution of ≤ 0.7 cm^{-1}.

Results and Discussion

Figure 1 reports the comparison between XRD powder diffraction lines (Figure 1a) and Raman spectra (Figure 1b) for different TiO_2 samples; the reference sample is the precursor powder TO.pre that has been subjected either to hydrothermal treatments, varying the aging time t_{HG} (72, 144, 552 h, samples labeled as TOHG72, TOHG144, TOHG552, respectively), or to direct calcinations at different temperatures (300 °C, TO.300; 600 °C, TO.600).

The diffraction pattern of the reference (TO.pre, fourth strip from the top in the figure) shows that the xerogel particles are amorphous. The presence of a very low, broad hump in the diffraction line apparent in the region of the rutile maximum intensity peak (∼27.5°) proves that, in agreement with literature results,[12] the spatial organization of the amorphous titanium hydrous oxide is closer to the rutile structure than to the anatase structure. The corresponding Raman curve of TO.pre in the 200−900 cm^{-1} region denotes the presence of three characteristic broad bands centered at about 398, 518, and 640 cm^{-1}. These bands can be attributed to the E_g, A_{1g}, and E_g vibration modes of anatase crystallites, respectively.[13] However, the broad band at about 210 cm^{-1} and the broad shoulders of the anatase E_g modes (at about 450 and 650 cm^{-1}) can be assigned to the presence of amorphous (rutile) phases.[14,15] Apparently, by means of Raman spectroscopy, both the bulk features apparent in the XRD lines and the initial local organization of the material toward the anatase structure are evidenced. Indeed, the Raman spectrum of the precursor calcined at 300 °C (TO.300) shows no appreciable bands relative to the amorphous (rutile) phase but only the three characteristic anatase peaks; the presence of the anatase peak at about 25.3° in the XRD pattern is fully consistent. The Raman curve of the sample calcined at 600 °C (TO.600) also shows, together with the anatase peaks, strong bands (B_{1g} at 210, E_g at 448, A_{1g} at 613, B_{2g} at 820 cm^{-1}) attributable to the rutile phase.[16] The rutile phase is appreciable also in the XRD spectrum (TO.600).

The Raman spectra of the samples hydrothermally grown at different t_{HG} (TOHG72, TOHG144, TOHG552) present both the anatase and brookite vibration modes (B_{1g} at 320, B_{2g} at 364, B_{2g} at 396 cm, and A_g at 636 cm^{-1}).[17] The sharpness of the anatase peaks increases with the length of the hydrothermal treatment. Such a conclusion is consistent with the XRD results: all the spectra show the contemporaneous presence of anatase and metastable brookite diffraction lines, and the increasing crystallinity of the aged samples with t_{HG}. The presence of a minor brookite peak at 31° (2q) was previously observed in the case of titania submitted to hydrothermal processing.[10]

The analysis of the Raman spectra (Figure 2) in the low wavelengths region (220−120 cm^{-1}) can give an estimation of the average diameter of the TiO_2 particles. Actually, in nanosized crystals, the breakdown of the Raman selection rule occurs and all the phonons in the whole Brillouin zones contribute to the Raman lines. In the case of TiO_2 particles, the confinement effect can be observed in the Raman position and shape of the E_g mode at 144 cm^{-1}. With decreasing of the diameter of the particles, the maximum of the Raman peak, corresponding to the E_g vibration mode, shifts to higher wavelength values (from

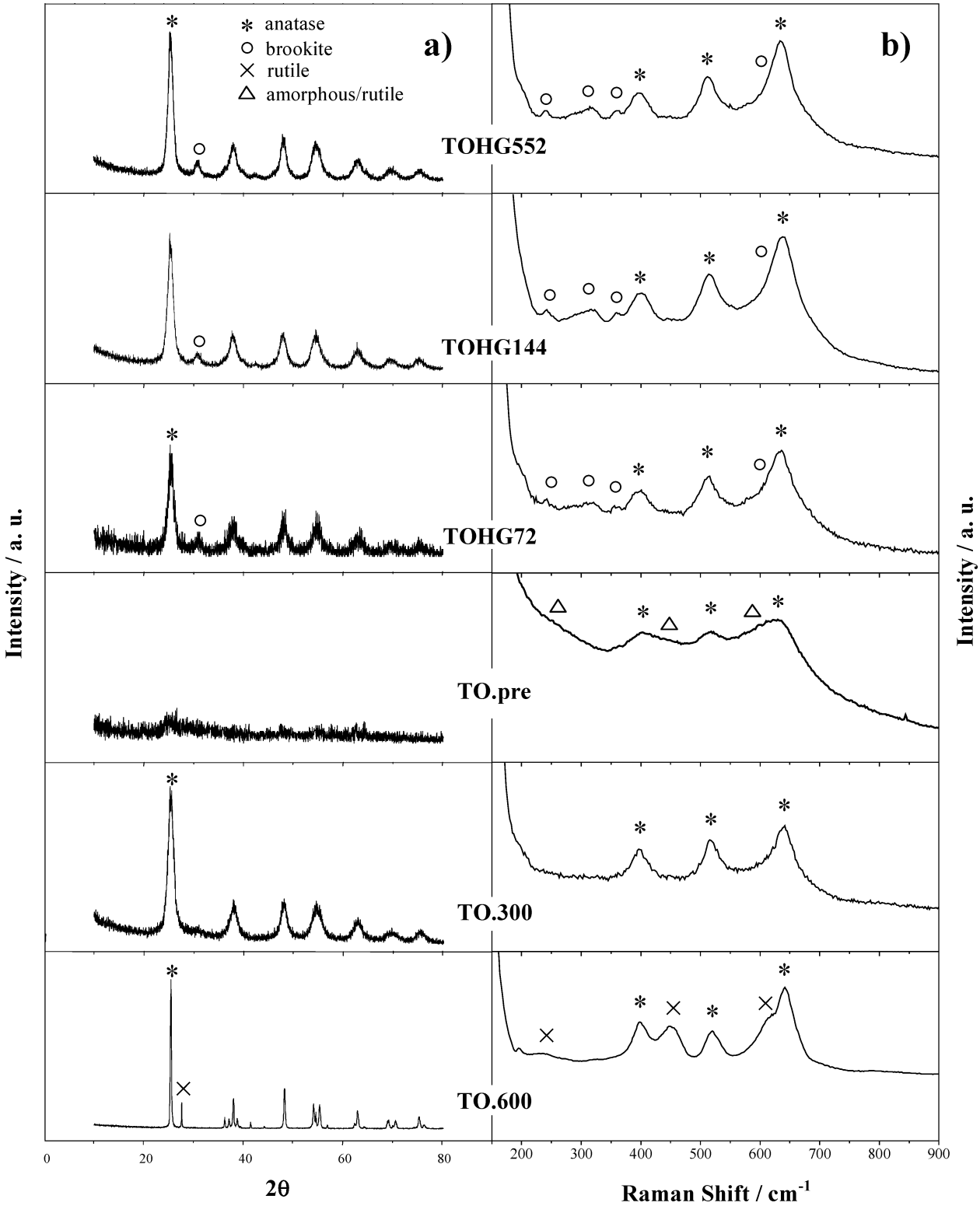

Figure 1. (a) Powder X-ray diffraction lines and (b) Raman spectra of precursor (TO.pre), hydrothermally grown (TOHG72, TOHG144, TOHG552), and calcined (TO.300, TO.600) samples.

144 to 153 cm^{-1}). Consequently, a broadening of the same vibration mode and an increase of the asymmetry toward higher wavelength values can be appreciated. The diameter of the TiO_2 particles can be evaluated by a model proposed by Campbell[18] and developed by Bersani.[19] Figure 2 shows the progressive shift of the Raman E_g mode that can be related to an increase in the diameter of the anatase crystallites with the time of hydrothermal growth ($7 < d < 10$ nm) and with the temperature of calcination ($d = 7-10$ nm at 300 °C, $d = 50$ nm at 600 °C). It is worthwhile to underline that the diameter of the particles, calculated by Scherer's equation using the fwhm of the most intense X-ray peak of anatase phase (inset to Figure 2), is fully comparable to the one obtained by Raman characterization.

Specific surface area values as a function of t_{HG} are reported in Figure 3. The length of the hydrothermal growth provokes a dramatic decrease in surface area with respect to the un-aged precursor (TO.pre) especially for short t_{HG}. Presumably, during the hydrothermal step, dissolution/reprecipitation mechanisms

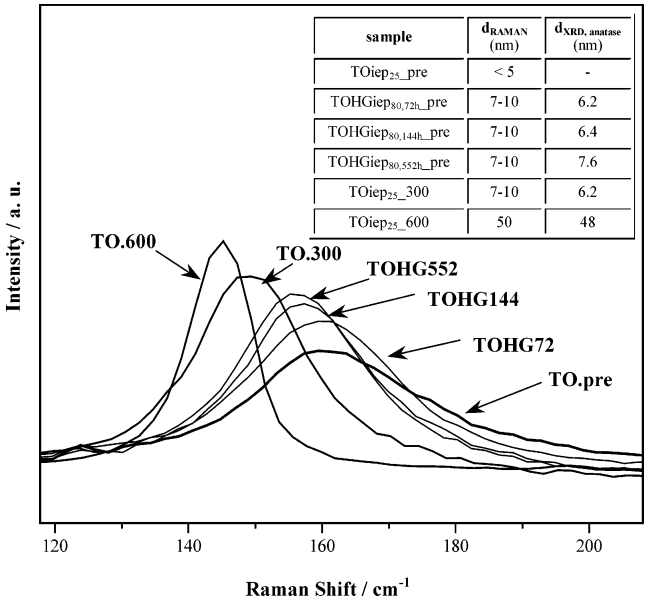

Figure 2. Raman spectra of E_g mode of anatase phase in the lowest-frequency region: shift in TiO−H stretching mode is a function of the aging time (TOHG72, TOHG144, TOHG552) and of the calcination temperature (TO.300, TO.600). (Inset) Corresponding diameter of the particles calculated by Raman (d_{RAMAN}) and XRD ($d_{XRD,anatase}$) fwhm of the anatase peak.

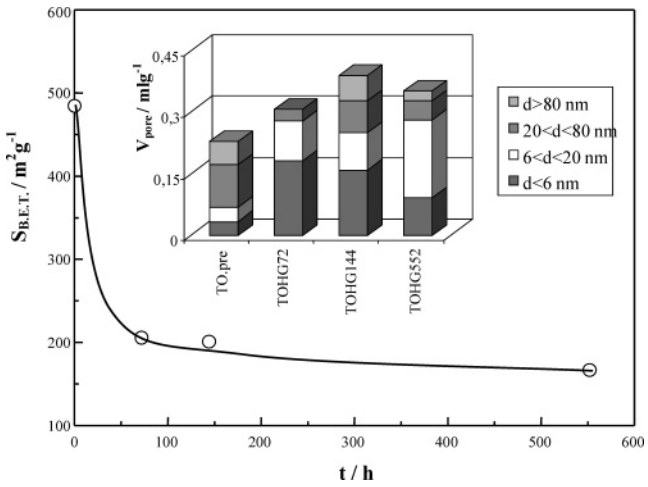

Figure 3. BET surface area as a function of aging time. (Inset) Total pore volume and pore size volume distribution of precursor (TO.pre) and aged samples (TOHG72, TOHG144, TOHG552).

(Ostwald ripening) take place, leading to a huge decrease in the surface area, the more so during the initial stages when the particles are mainly polidispersed. Very interesting is also the comparison of the total pore volumes and the respective distribution in the different pore sizes of the aged samples and of the un-aged xerogel (inset to Figure 3). In the case of the samples aged for 72, 144, 552 h, the total pore volume is larger than that of the un-aged one, and the amount of pores with small and intermediate diameters ($6 < d < 20$ nm) increase with the time of the hydrothermal treatment. For all the samples, the shape of the nitrogen adsorption isotherm hysteresis loops[12] suggests the occurrence of pores with an average bottleneck shape.

The comparison between the experimental surface area and the S_{calc} from X-ray diffraction data (Table 1) shows that, in the case of the samples hydrothermally treated (TOHG72, TOHG144, TOHG552), the actual particles can be considered to be mainly composed of single crystals. On the contrary, the

TABLE 1: Comparison between Experimental (S_{BET}) and Calculated (S_{calc}) Surface Areas for Precursors (TO.pre), Aged Samples (TOHG72, TOHG144, TOHG552), and Calcined Samples (TOHG552.300, TOHG552.600, TO.300, TO.600)

sample	S_{BET} m^2 g^{-1}	S_{calc} m^2 g^{-1}
TO.pre	484.7	
TOHG72	205.4	196
TOHG144	200.5	195
TOHG552	166.5	166
TOHG552.300	155.5	170
TOHG552.600	43.3	58
TO.300	182.3	202
TO.600	10.3	26

values of the S_{BET} of the samples calcined at 300 and 600 °C are lower than the calculated ones; in the case of TO.600, the particles can be definitely considered the result of the sintering of several crystallites.

To understand the effects of the hydrothermal step on the formation of the titania phases, the outcome of calcinations performed either directly on the precursor (TO.pre) or on the precursor aged for 552 h (TOHG552) can be considered (Figure 4). The expected decrease of the sample surface area with the temperature of calcination is different between the aged (TOHG552) and the reference (TO.pre) sample; in the case of the powder hydrothermally grown for 552 h, the contraction of the S_{BET} with the temperature is much less abrupt than for that of the precursor (TO.pre). Further, the contraction in surface area upon heating at 600 °C is much lower for the aged precursor, the surface area of TOHG552.600 being about four times that of TO.600.

Figure 5 shows the corresponding Raman spectra of the two series of calcined samples, TO.300 and TO.600, and TO552.300 and TO552.600. The effect of the aging time before the calcination provokes the appearance of the brookite phase in both samples calcined at 300 and 600 °C. It is worthwhile to underline that the rutile phase, evident in the TO.600 sample, is no more appreciable in the sample hydrothermally grown for 552 h and calcined at the same temperature. These results are in full agreement with the quantitative phase compositions obtained by XRD determinations (Table 2). The larger surface area of the TO552.600 sample (see Table 1) can be possibly related to the inhibition of the rutile formation in this sample with respect to TO.600. The direct calcination of the amorphous embryos of the precursor leads to a sintered product (see Tab.1). Particle arrangement and packing is reported to influence the thermal stability and phase transformation of materials. Banfield et al.[11] reported that the anatase−rutile transformation could be initiated from the rutile-like elements created at the oriented contacts between anatase particles. The lack of proper particle attachment or particle coordination would instead decrease the possibility of rutile nucleation. The looser packing of particles generated in the hydrothermal treatment might be one of the main factors responsible for the higher thermal stability of the anatase structure.

The pore size distribution of the different samples (Figure 6) reflects consistently the above arguments. The TOHG552 sample shows the largest presence of small interparticle mesopores, which are mantained, although to a lesser extent, in the 600 °C calcined aged sample (TOHG552.600).

The knowledge of the surface network and, in particular, of the distribution and kind of hydroxyls species by using Raman spectroscopy[20] is a key point to clarify the role played by water in the hydrothermal steps. Figure 7 reports the Raman spectrum of the precursor (TO.pre) in a wide wavelength range (1300−

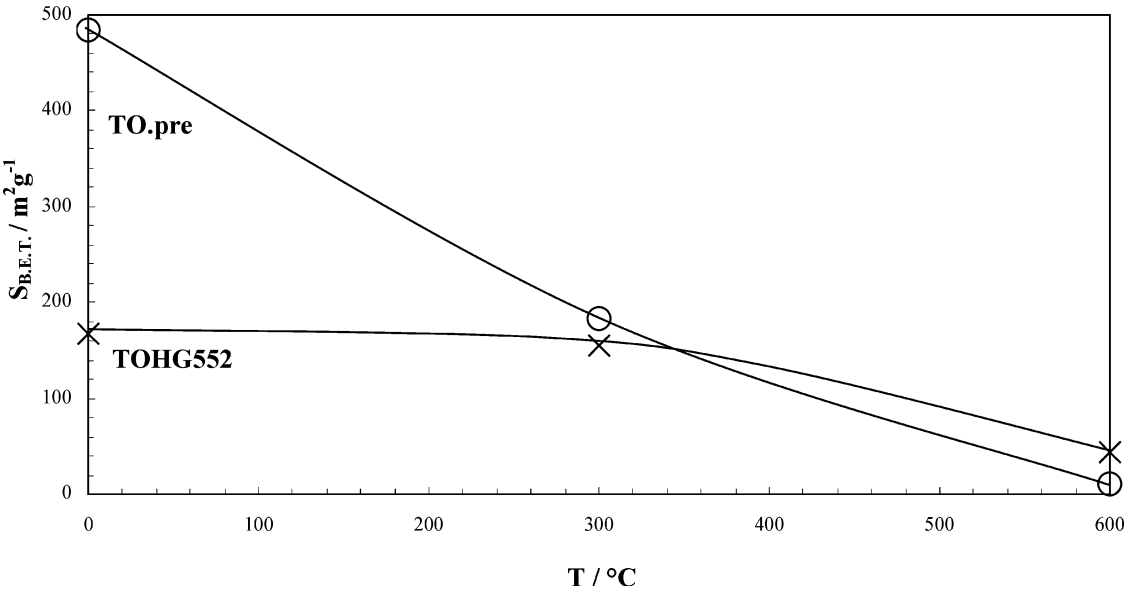

Figure 4. BET surface area of precursor (TO.pre) and aged sample (TOHG552) as a function of the calcination temperature.

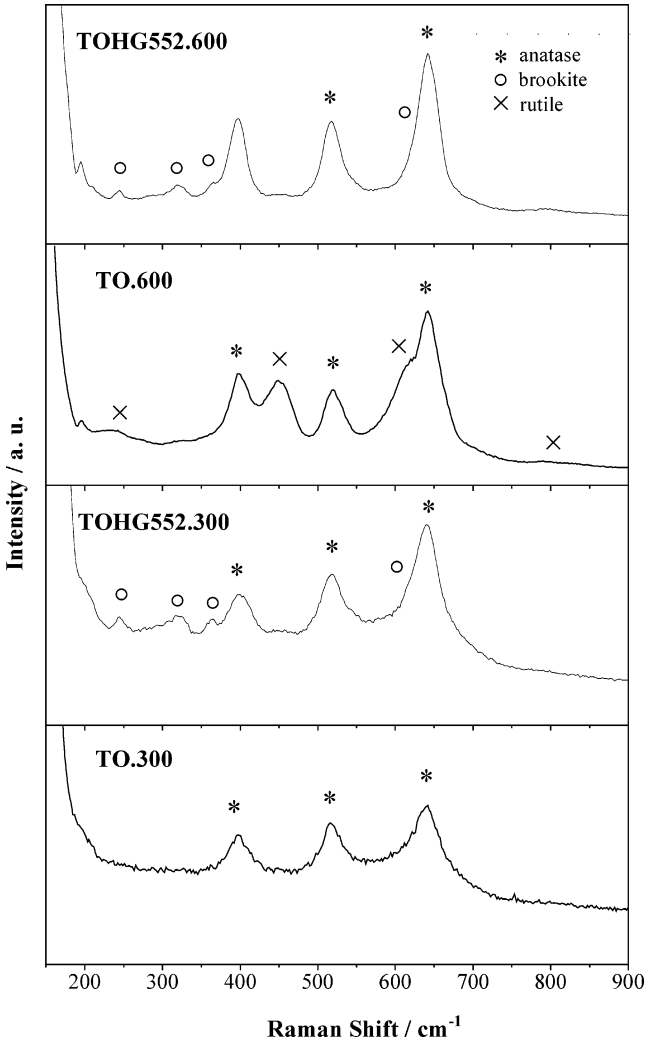

Figure 5. Raman spectra of calcined precursor (TO.300, TO.600) and of the calcined aged sample (TOHG552.300, TOHG552.600).

3900 cm^{-1}). The presence of a small peak at 1630 cm^{-1} can be attributed to the bending vibration mode of the adsorbed OH anions on the TiO_2 surface.[29,30] The broad peak in the water −OH stretching region (2700−3900 cm^{-1}) can be fitted (inset)

TABLE 2: Quantitative Phase Composition[a] and Relative Anatase Diameter of Calcined Samples

sample	% A	% B	% R	d_A (nm)
TO.300	96.5	3.5		6.2
TO.600	86.8		13.2	48.4
TOHG552.300	75.4	24.6		7.4
TOHG552.600	98.2		1.8	21.7

[a] A = anatase, B = brookite, and R = rutile

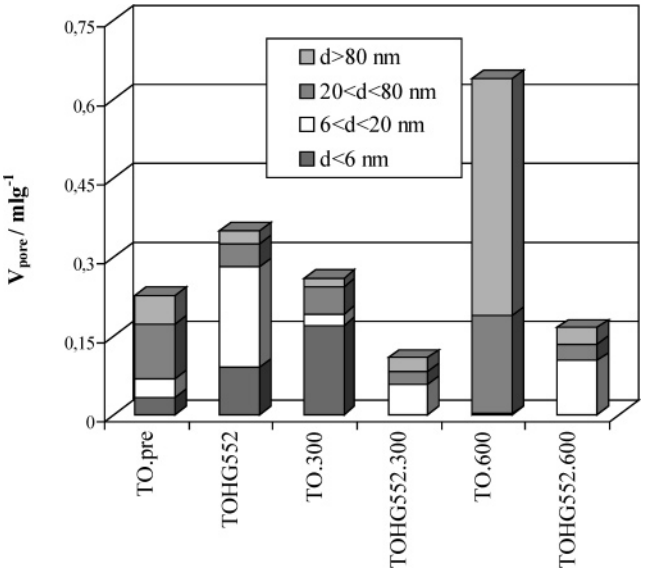

Figure 6. Total pore volume and pore size volume distribution of precursor (TO.pre) aged (TOHG552) and calcined sample (TO.300, TOHG552.300, TO.600, TOHG552.600).

on the grounds of different contributions:[20] (i) curve (a) corresponds to the free liquid water (O−H stretching),[20] obtained by the superposition of three different bands at 3250, 3451, and 3608 cm^{-1}; (ii) curve (b) can be assigned to O−H stretching in adsorbed water dimers[20] peaked at 3008 cm^{-1}; (iii) curve (c) has been associated with the TiO−H stretching of the surface titanols hydrogen bonded to molecular water (3335 cm^{-1});[20−28] (iv) in curve (d), O−H stretching in adsorbed water[20] at the surface and mutually hydrogen-bonded TiO−H stretching of surface hydroxyls have been attributed to the vibration peaked at 3544 cm^{-1}.

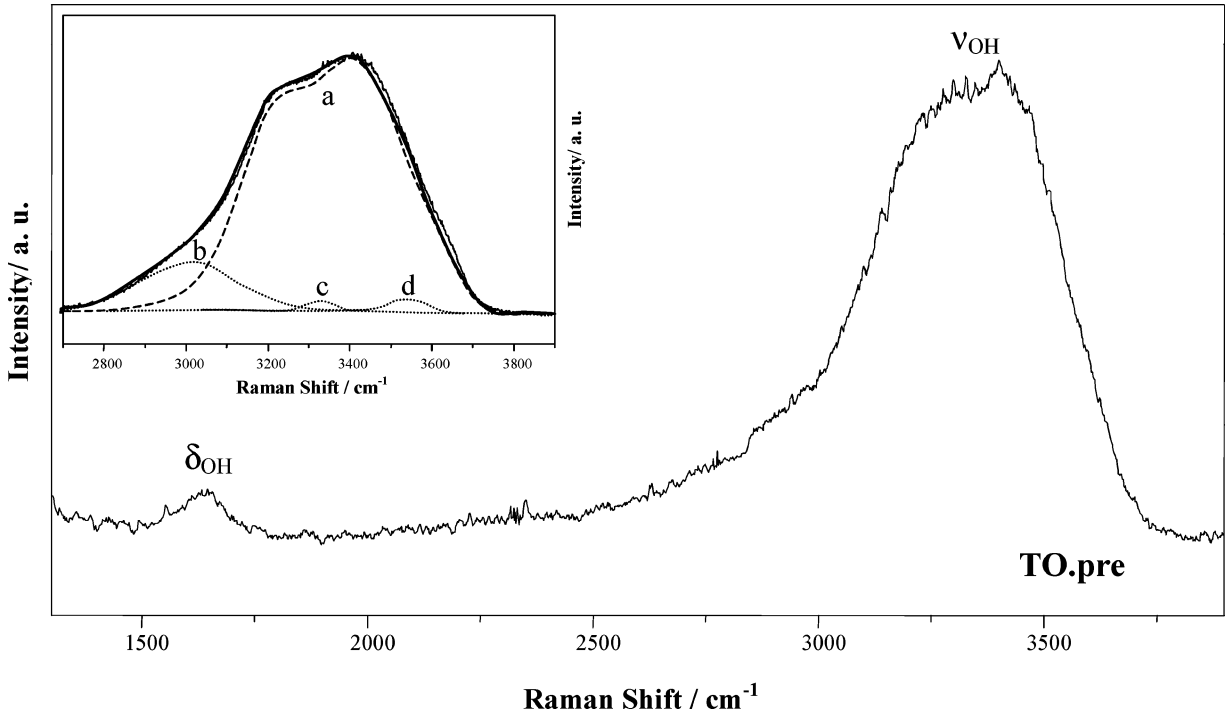

Figure 7. Raman spectra of the precursor sample (TO.pre) in the region 1500−4000 cm^{-1}. (Inset) Best fit deconvolution in the water O−H stretching region (2700−3900 cm^{-1}): dashed, dotted lines are the Gaussian components according to the fitting analysis, and the solid line is the resulting fit.

The water vibration pattern apparent for the precursor (Figure 7) does not undergo general modifications either in the case of the 552 h hydrothermal sample or that of the 300 °C calcinated sample (Figure 8a). The hydrothermal sample shows, however, a larger amount of free liquid water. In this case, instead of the direct heating of the precursor at 600 °C (TO.600), the contribution of the OH stretching of free liquid water is totally absent and only a small contribution due to the adsorbed water can be still estimated. The marked decrease of the H_2O stretching bands and the corresponding presence of the H_2O bending mode can be associated with the highly structured configuration of chemisorbed water.[14,31] The calcination at 600 °C of the sample hydrothermally grown (TOHG552.600) instead does not provoke the total removal of the free water; the ν_{OH} Raman bands in the 2900−3700 cm^{-1} region being still appreciable.

The residual presence of free water at the surface of the TOHG552.600 is fully consistent with the higher thermal stability shown by the 552 hydrothermal sample, already discussed with reference to the phase composition and surface area.

Conclusions

TiO_2 hydrous precursors, prepared by following a sol−gel preparative route, were submitted to hydrothermal steps at room pressure for increasing time lengths. During the hydrothermal step, particle growth occurs via dissolution/reprecipitation mechanisms, leading to single-crystal anatase particles with crystallites in the range of 6−8 nm. Elaboration of Raman spectra in the low wavelengths region leads to crystallite sizes that are almost coincident with the ones obtained by XRD, suggesting the formation of an ordered material in which long range and local structures are alike. In the case of the un-aged precursor, instead, the starting microstructures of anatase were appreciable only by means of Raman spectroscopy, while XRD gave indications of a fully amorphous system.

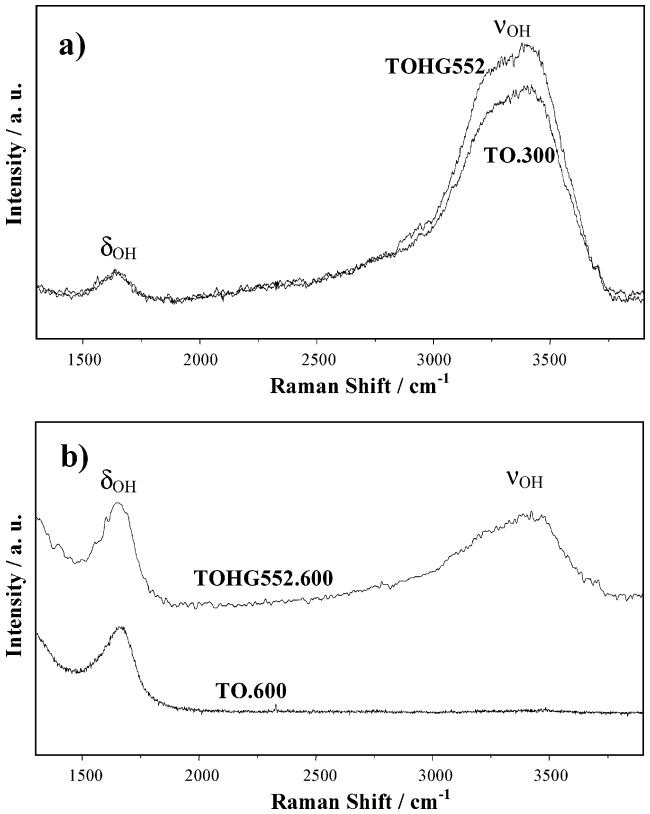

Figure 8. Comparison between Raman spectra in the region 1500−4000 cm^{-1} of (a) precursor calcined at 300 °C (TO.300) and aged sample for 552 h (TOHG552); (b) precursor calcined at 600 °C (TO.600) and hydrothermally treated sample for 552 h, calcined at the same temperature (TOHG552.600).

The effects provoked by thermal treatments at 600 °C were found to be markedly affected by the structural and textural features of the starting powders. Direct heating of the amorphous

phase leads to the formation of a low surface area material where a severe sintering between the pristine particles supported the formation of appreciable amounts of rutile in mixture with anatase. Calcination of the nanocrystalline aged precursor leads instead to an almost pure anatase TiO_2 (rutile lower than 2%) with crystallite sizes of about 20 nm, a larger surface area and an appreciable extent of mesopores. The analysis of the water oxide interactions by Raman scattering shows that the 600 °C heating of the un-aged precursor provokes to total removal of free water, while for the aged sample, a broad peak in the OH stretching region indicates the residual presence of free water.

As a general consideration, it can be concluded that the present procedure might be suggested as a synthetic path for titanium dioxide to be used in photovoltaic systems. In fact, the present combination of aging steps, performed in mild conditions with the opportune selection of the sol−gel parameters, has led to ordered anatase nanocrystalline powders of 6−8 nm with large surface area and small interparticle mesopores. The interfacial reactivity and excellent wettability are ensured by the large amount of free water as apparent from the peak in the OH stretching region of Raman spectra.

Acknowledgment. Financial support from the Ministry of Education, University, and Research (MIUR, FIRST Funds) is gratefully acknowledged.

References and Notes

(1) Boiadjieva, T.; Cappelletti, G.; Ardizzone, S.; Rondinini, S.; Vertova, A. *Phys. Chem. Chem. Phys.* **2003**, *5*, 1689.

(2) Matsuda, A.; Kotani, Y.; Kogure, T.; Tatsumisago, M.; Minami, T. *J. Am. Ceram. Soc.* **2000**, *83*, 229.

(3) Traversa, E.; Di Vona, M. L.; Licoccia, S.; Sacerdoti, M.; Carotta, M. C.; Crema, L.; Martinelli, G. *J. Sol.-Gel Sci. Technol.* **2001**, *22*, 167.

(4) Wilson, G. J.; Will, G. D.; Frost, R. L.; Montgomery, S. A. *J. Mater. Chem.* **2002**, *12*, 1787.

(5) Barbè, C. J.; Arendse, F.; Comte, P.; Jirousek, M.; Lenzmann, F.; Shklover, V.; Graetzel, M. *J. Am. Ceram. Soc.* **1997**, *80*, 3157.

(6) Kato, K.; Tsuzuki, A.; Taoda, H.; Torii, Y.; Kato, T.; Butsugan, Y. *J. Mater. Sci.* **1944**, *29*, 5911.

(7) Kotani, Y.; Matsuda, A.; Tatsumisago, M.; Minami, T.; Umezawa, T.; Kogure, T. *J. Sol.-Gel Sci. Technol.* **2000**, *19*, 585.

(8) Kavan, L.; Graetzel, M.; Rathousky, J.; Zukal, A. *J. Electrochem. Soc.* **1996**, *143*, 394.

(9) Chen, Y. F.; Lee, C. Y.; Yeng, M. Y.; Chiu, H. T. *Mater. Chem. Phys.* **2003**, *81*, 39.

(10) Wang, C. C.; Ying, J. Y. *Chem. Mater.* **1999**, *11*, 3113.

(11) Penn, R. L.; Banfield, J. F. *Geochim. Cosmochim. Acta* **1999**, *63*, 1549.

(12) Boiadjieva, T.; Cappelletti, G.; Ardizzone, S.; Rondinini, S.; Vertova, A. *Phys. Chem. Chem. Phys.* **2004**, *6*, 3535.

(13) Zhang, W. F.; He, Y. L.; Zhang, M. S.; Yin, Z.; Chen, Q. *J. Appl. Phys.* **2000**, *33*, 912.

(14) Chen, Y. F.; Lee, C. Y.; Yeng, M. Y.; Chiu, H. T. *J. Cryst. Growth* **2003**, *247*, 363.

(15) Ocana, M.; Garcia-Ramos, J. V.; Serna, C. J. *J. Am. Ceram. Soc.* **1992**, *75*, 2010.

(16) Robert, T. D.; Laude, L. D.; Geskin, V. M.; Lazzaroni, R.; Gouttebaron, R. *Thin Solid Films* **2003**, *440*, 268.

(17) Tompsett, G. A.; Bowmaker, G. A.; Cooney, R. P.; Metson, J. B.; Rodgers, K. A.; Seakins, J. M. *J. Raman Spectrosc.* **1995**, *26*, 57.

(18) Campbell, I. H.; Fauchet, P. M. *Solid State Commun.* **1986**, *85*, 73.

(19) Bersani, D.; Lottici, P. P.; Ding, X. Z. *Appl. Phys. Lett.* **1998**, *72*, 73.

(20) Anedda, A.; Carbonaro, C. M.; Clemente, F.; Corpino, R.; Ricci, P. C. *J. Phys. Chem. B* **2003**, *107*, 13661.

(21) Glinka, Y. D.; Lin, S. H.; Chen, Y. T. *Phys. Rev. B: Condens. Matter Mater. Phys.* **2000**, *62*, 4733.

(22) Brinker, J.; Scherer, G. W. *Sol-Gel Science: The Physics and Chemistry of Sol-Gel Processing*; Academic Press: San Diego, 1990.

(23) Klein, L. C.; Gallo, T. A.; Garvey, G. J. *J. Non-Cryst. Solids* **1984**, *63*, 23.

(24) Gottardi, V.; Guglielmi, M.; Bertoluzza, A.; Fagnano, C.; Morelli, M. A. *J. Non-Cryst. Solids* **1984**, *63*, 71.

(25) Kinowski, C.; Bouazaoui, M.; Bechara, R.; Henc, L. L.; Nedelec, J. M.; Turrell, S. *J. Non-Cryst. Solids* **2001**, *291*, 143.

(26) Davis, K. M.; Tomozawa, M. *J. Non-Cryst. Solids* **1996**, *201*, 177.

(27) Morrow, B. A.; McFarlan, A. J. *J. Phys. Chem.* **1992**, *96*, 29.

(28) Benesi, H. A.; Jones, A. C. *J. Phys. Chem.* **1959**, *63*, 179.

(29) Rull, F. *Pure Appl. Chem.* **2002**, *74*, 1859.

(30) Tominaga, Y.; Fuyiwara, A.; Amo, Y. *Fluid Phase Equilib.* **1998**, *144*, 323.

(31) Ninness, B. J.; Bousfield, D. W.; Tripp, C. P. *Colloids Surf., A* **2003**, *214*, 195.